Neural coding of choice and outcome are modulated by uncertainty in orbitofrontal but not secondary motor cortex

Juan Luis Romero-Sosa[1], Andrew M. Wikenheiser[1-3], Hugh T. Blair[1-3#] & Alicia Izquierdo[1-4#]

[1]Department of Psychology, University of California-Los Angeles, Los Angeles, California, USA.

[2]The Brain Research Institute, University of California-Los Angeles, Los Angeles, California, USA.

[3]Integrative Center for Learning and Memory, University of California-Los Angeles, Los Angeles, California, USA.

[4]Integrative Center for Addictions, University of California-Los Angeles, Los Angeles, California, USA.

#co-supervised this work

Corresponding authors:

Juan Luis Romero-Sosa jromero12@ucla.edu and

Dr. Alicia Izquierdo aizque@ucla.edu

Abstract

Orbitofrontal cortex (OFC) and secondary motor cortex (M2) are both implicated in flexible reward learning but the conditions that differentially recruit these regions are not fully understood. We imaged calcium activity from single neurons in OFC or M2 during *de novo* learning of uncertain reward probability schedules. After controlling for experience, predictions of choice were decoded from M2 neurons with similar accuracy under all certainty conditions, but were more accurately decoded from OFC neurons under greater uncertainty. In M2, the proportion of outcome selective neurons decreased with uncertainty whereas this proportion remained stable in OFC, due to an increased recruitment of reward-selective neurons across levels of uncertainty. Decoding accuracy of both choice and outcome were positively correlated with indices of flexible strategy use in OFC, but not M2. Our results indicate that OFC neurons preferentially encode choices and outcomes under conditions of uncertainty that foster greater reliance on adaptive strategies.

INTRODUCTION

Both the orbitofrontal cortex (OFC) and secondary motor cortex (M2) are involved in flexible reward learning and reward-motivated decision making. M2 receives dense inputs from diverse cortices, including sensorimotor, visual, retrosplenial, and orbital regions [1], and in turn, sends projections to striatum that fall along mediolateral and rostrocaudal gradients within M2 [2], enabling precise control of actions. This anatomical connectivity positions M2 well to control action flexibly based on both sensory and motivation information. Functional studies have determined that M2 is essential for action updates [3] and that it enables the flexible assignment of either stimuli or motor antecedents to action plans [4-6]. Additionally, there has been discovery of different population dynamics in M2 depending on the strategy and stimulus modality that mice use in a flexible decision-making task [7]. Given its integration of sensory and motivation evidence, M2 has an essential role in higher-order movement control and orienting [8] but can also bias choice based on outcomes and choice history [9, 10]. Though a previous electrophysiological study indicated orbitofrontal cortex (OFC) is involved in updating outcome value from prior actions [11], authors found that M2 signaled choice earlier than any other area of rat frontal cortex, and remarkably also contained a value signal [12].

OFC also has a well-substantiated role in flexible decision making [13-16]. Several groups have reported choice-predictive neurons in OFC in equivalent or even larger numbers than value or outcome-encoding cells in this region [17-21]. One group found that over half of the neurons they recorded in OFC encoded both the direction of choice and the location of the goal, concluding that choice selective neurons in OFC represent spatial-motor information required to define specific goals and necessary actions to obtain them [21]. However, it is presently unclear if and how these representations change with uncertainty. A somewhat parallel literature suggests OFC may be critically involved in learning, especially under uncertain or probabilistic conditions [22-24], where it may set the expectation for the rest of learning [25-28]. This is consistent with the idea that OFC stores long-term action values [25, 29], stimulus values [30], and causally contributes to an 'expected uncertainty' or baseline risk in rats [31, 32]. This risk is signaled by single neurons in OFC in rats [33, 34] and in nonhuman primates [35, 36]. One study [37] reported that OFC neurons track expectations across a slow timescale (i.e., across-session probabilistic reversal learning) and are also recruited for trial-by-trial learning, or value updates, on a fast timescale (i.e., within a session). However, this study did not manipulate the reward uncertainty over time. Critically, aside from the Hattori et al. (2023) study, recording and imaging studies in both rodent and primate species typically assess the role of OFC in decisions in expert animals,

not during the learning of risk or expected uncertainty. Thus, it is unknown how choice and outcome cell selectivity may change over the course of learning, especially with increasing uncertainty in OFC. All of the above suggests that although M2 and OFC are involved in flexible learning and decision-making, their involvement could dissociate over different timescales and increasingly uncertain conditions.

Using miniscopes, we compared populations of neurons and single cells in OFC and M2 over several sessions of learning in freely-behaving rats. Unlike the great number of studies assessing these regions in well-trained animals, here we studied calcium dynamics during *de novo* learning. We were primarily interested in determining if and when neural dynamics would differentially predict choice and outcome in M2 vs. OFC, and which behavioral and task features single cells were selective for in these regions across learning under uncertainty.

RESULTS

Learning under increasing uncertainty

Male and female Long–Evans rats first underwent stereotaxic surgery to infuse GCaMP6f into either M2 or OFC (see Methods). In the same surgery, a GRIN lens was unilaterally implanted over the site of the viral infusion (**Figure 1D-F**; photomicrographs of lens implant and calcium indicator expression for all rats are shown in **Supplementary Figure 1**). Following surgical recovery and baseplating, rats then underwent pretraining followed by six sessions of learning. In a touchscreen-outfitted chamber, rats were required to initiate each trial by touching a center stimulus and then make a choice to touch a stimulus on either the left or right side. If correct, rats could retrieve a sucrose pellet reward from a food port located on the opposite side of the touchscreen response zone, signaled by a light cue in the port. This visual cue appeared concurrently with pellet delivery on rewarded, but not unrewarded, trials. The reward contingencies reversed every 75 trials and increased in uncertainty on the last block of trials, with reward schedules progressing from less to more reward uncertainty (100:0 to 70:30) (**Figure 1A-B**). The probability of reward delivery depended on the rat's choice (left vs. right), with one side delivering a higher probability of reward than the other. Each session consisted of 3 blocks of 75 trials (225 trials total); the response with the highest reward probability (left vs. right) was reversed at the start of each block. Within each session, the probability ratio remained the same for the first two trial blocks and then changed to a ratio with higher uncertainty for the last block of trials. As shown in **Figure 1C**, sessions 1 and 2 used a ratio of 100:0 for blocks 1-2 and 90:10 for block 3 (Schedule 1), sessions 3 and 4 used a ratio of 90:10 for blocks 1-2 and 80:20 for block 3 (Schedule

2), and sessions 5 and 6 used a ratio of 80:20 for blocks 1-2 and 70:30 for block 3 (Schedule 3). **Figure 1G** shows an example of a single rat's performance during a Schedule 2 session.

Results of an omnibus Generalized Linear Model (GLM) on predictors of accuracy are found in **Table 1**. Rats tended to improve across all trials (GLM: $\beta_{trialnum} = 0.01$, $p < 0.01$) while performance expectedly dipped on block switches when reversals occurred (GLM: $\beta_{block} = -0.439$, $p < 0.01$), **Figure 1H**. We found there were no significant differences in lens implant location on learning accuracy as measured by probability correct (**Table 2**).

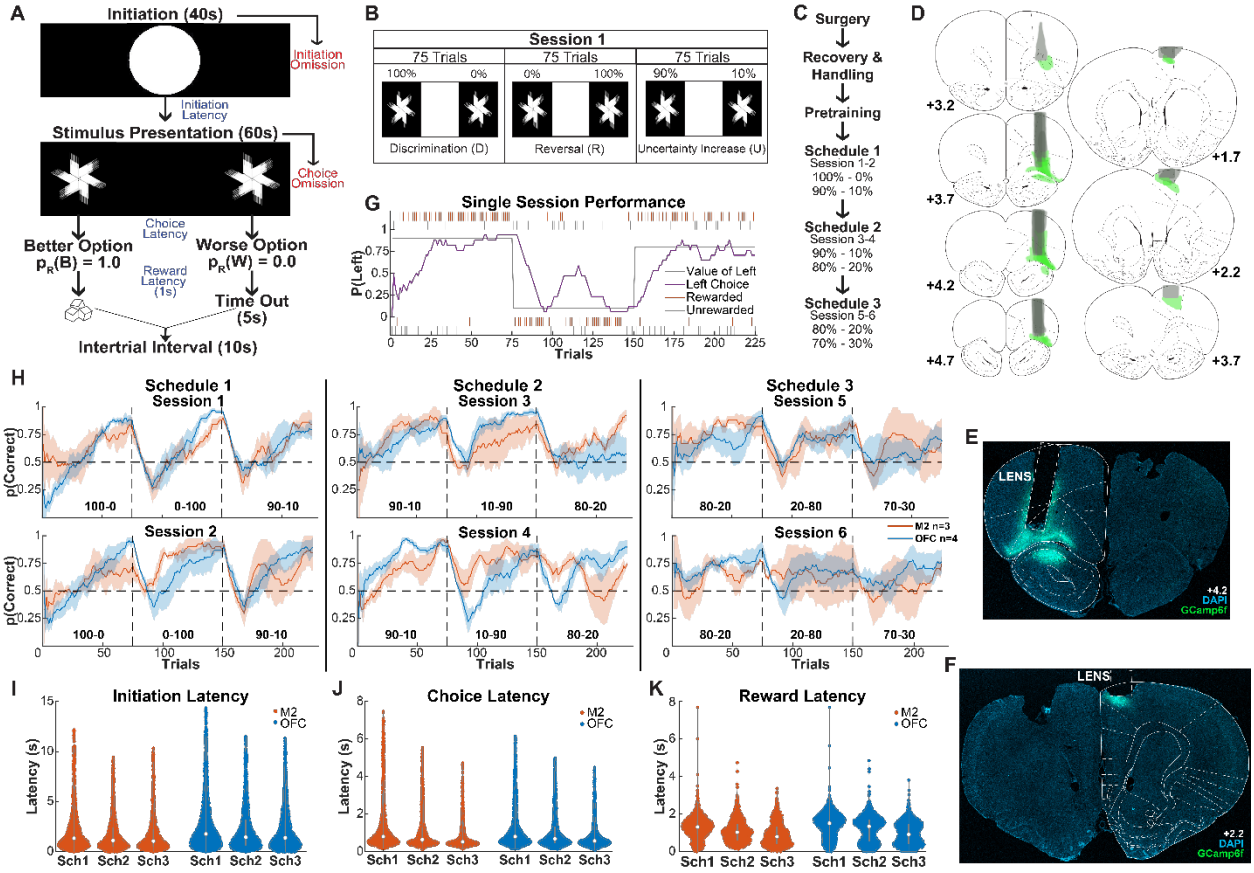

Figure 1. Restless bandit task performance in freely-behaving, lens-implanted rats. (A) Schematic of trial timeline: Rats learn in an operant chamber outfitted with a touchscreen with three different interaction zones (left, center, and right) and a reward port on the opposite side of the chamber. A white circle is presented in the middle zone for 40 seconds, during which the rat is required to nosepoke to initiate a trial. Subsequently, two identical stimuli are presented on the left and right side of the screen for 60 seconds. The rat is required to nosepoke one of these stimuli, selecting either the left or right side. One of the sides has a higher reward probability than the other. The rat either gets rewarded 1 s after the nosepoke or undergoes a 5-second timeout. There is a 10 second Intertrial Interval (ITI) before a new trial begins. **(B)** A session consists of 3 blocks of 75 trials each, with two reversals, with the last block increasing in uncertainty. **(C)** Following surgery, recovery, handling, and pretraining to respond to touchscreen stimuli on either the left or the right, different schedules are introduced, with each schedule administered across two days each, and increasing in uncertainty. **(D)** Reconstructions of calcium indicator GCaMP6f and GRIN lens implant in all rats. **(E)** Photomicrograph of a lens in OFC. **(F)** Photomicrograph of a lens in M2. **(G)** Sample performance on Schedule 2 where the rat matches the value of the left side and adapts its behavior following a reversal. **(H)** There was no significant difference in accuracy, or p(Correct), by lens implant area (**Table 1**). **(I-K)** Performance measures by lens implant region to include latencies for Initiation **(I)**, Choice **(J)**, and Reward **(K)** for M2- and OFC-lens implanted rats across all the schedules.

Though rats with lens implants in M2 vs. OFC did not differ in their acquisition rates (**Table 5**), compared with a sham control group, implanted animals exhibited slightly attenuated learning compared to viral, non-tethered controls (GLM: $\beta_{Implanted_Lens} = -0.13$, $p < 0.01$, **Supplementary Figure 2, Supplementary Table 1**). For latency measures, non-tethered controls initiated trials and collected rewards more quickly but exhibited slower choice latencies (**Supplementary Tables 2-4**). Latencies to initiate trials and collect reward did not differ in M2- vs. OFC-implanted animals, but choice latencies were faster in the OFC-implanted animals than in the M2-implanted animals (GLM: $\beta_{Area} = -0.57$, $p < 0.01$, **Figure 1I-K**, **Tables 2-4**).

Decoding choice from calcium activity

Binary support vector machine (SVM) classifiers were trained to predict *Chosen Side* (left vs. right) from calcium traces aligned to the choice nosepoke (**Figure 2A-B)**. To determine the most appropriate windows for statistical analysis, we generated peak-aligned heatmaps and found cells that exhibited time-locked activity to either choice or reward cue **(Figure 2D-E)**. Decoder training sets were balanced to include an equal number of rewarded/unrewarded and left/right trials across all schedules (**Figure 2C**). In both M2 and OFC, choice decoding accuracy ramped up from chance starting prior to trial initiation (suggesting that rats often anticipated which side they would choose prior to trial initiation), and peaked ~500 ms after choice (**Figure 2F**). An analysis of predictors of decoding accuracy in the bin just prior to choice (yellow shaded region in **Figure 2F**) resulted in more accurate decoding in M2 than OFC ($\beta_{Area} = -0.231$, $p = 0.0004$), with no effect of schedule ($\beta_{Schedule} = -0.0843$, $p = 0.19$), but a significant Area x Schedule interaction ($\beta_{Area:Schedule} = 0.056$, $p = 0.0475$), **Table 5**. *Chosen Side* was decoded from M2 with similarly high accuracy under all probability schedules, whereas decoding was more accurate in OFC when the schedule was more uncertain. Confirming this, post-hoc analyses on each schedule (**Table 6**) revealed that decoding from M2 was more accurate than from OFC under conditions of higher certainty (Schedule 1: $\beta_{Area} = -0.174$, $p = 0.0027$; Schedule 2: $\beta_{Area} = -0.119$, $p = 0.0438$), but under the least certain schedule, OFC decoding accuracy increased to become equivalent to M2 decoding accuracy (Schedule 3: $\beta_{Area} = -0.0621$, $p = 0.073$). This certainty-dependent decoding accuracy in OFC was not accounted for by experience (i.e., session) since experience was a covariate in the GLM model and was not a significant predictor of choice accuracy ($\beta_{Session} = 0.0268$, $p = 0.234$). Additionally, to check if the number of neurons used to train decoders affected decoder accuracy, we entered this variable as a moderator in the GLM. We did not find any significant effect or interaction with any other variable ($\beta_{NumCells} = -0.0008$, $p = 0.22$, $\beta_{NumCells:Area} =$

0.0008, p = 0.12, $\beta_{NumCells:schedule}$ = 0.0004, p = 0.17, $\beta_{NumCells:Area:schedule}$ = -0.0003, p = 0.19), indicating that ensemble size did not significantly explain decoder accuracy results.

Decoding outcome from calcium activity

SVM classifiers were trained to predict *Trial Outcome* (rewarded vs. unrewarded) from calcium traces aligned to the choice nosepoke (**Figure 2A-B**). At time points before the outcome was known (that is, prior to 1 second after the choice nosepoke), the accuracy of outcome decoding was limited by the certainty of the outcome (which was highest under Schedule 1 and

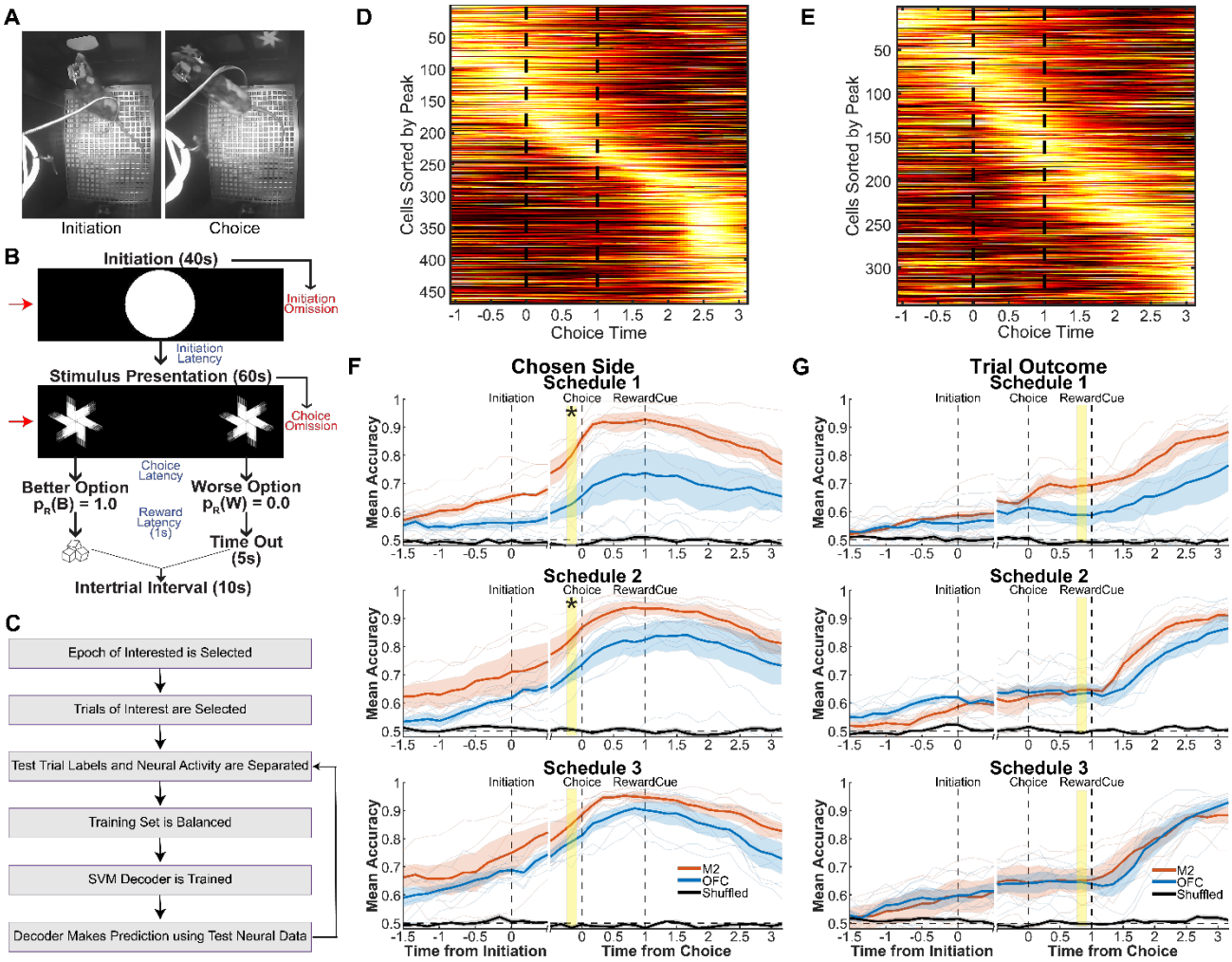

Figure 2. OFC, but not M2, choice decoding accuracy increases with uncertainty. **(A)** Trial epochs selected for analysis of neural data: Initiation (left) and Choice (right). **(B)** Same epochs in A, shown in the trial timeline. **(C)** A flowchart of how the decoder was trained with balanced data and then tested on each trial. **(D)** Example of a cross-validated peak-aligned heatmap aligned at choice from an imaging session in M2 during schedule 2. **(E)** Same as D but in OFC. **(F)** Decoder accuracy from an SVM binary decoder trained using balanced neural data from either M2 or OFC. The solid line is the mean and the shaded region is the standard deviation. The decoder was trained to predict whether the choice would be left or right (*Chosen Side*). We found a main effect of Area and Area x Schedule interaction, with post-hoc analysis revealing better decoding in M2 than OFC in Schedule 1 and 2, but not Schedule 3. Decoder accuracy using shuffled neural data in both M2 and OFC is shown in black. **(G)** Similar to F but here the decoder was trained to predict whether the trial would be rewarded or not (*Trial Outcome*). We found main effects of Area and Schedule, but no significant interaction of Area x Schedule. *p< 0.05.

lowest under Schedule 3). In both M2 and OFC, decoding accuracy for *Trial Outcome* began ramping up from chance at trial initiation and then stalled at a plateau which persisted until the outcome was known, after which decoding accuracy began ramping upward again (**Figure 2G**). A GLM analysis of decoding accuracy in the bin just prior to the outcome (yellow shaded region in **Figure 2G**) resulted in, as expected, better decoding of outcome for certain than uncertain schedules ($\beta_{Schedule}$ = -0.128, p = 0.0494). Decoding was also more accurate in M2 than OFC (β_{Area} = -0.138, p = 0.0248). There was similarly no effect of overall experience, or session number (**Table 7**). Here we also included the number of neurons as a moderator and again did not find a significant effect or interaction of ensemble size with any of the other predictors ($\beta_{NumCells}$ = -0.00001, p = 0.98, $\beta_{NumCells:Area}$ = 0.0002, p = 0.59, $\beta_{NumCells:schedule}$ = 0.0002, p = 0.34, $\beta_{NumCells:Area:schedule}$ = -0.0002, p = 0.31).

The ratio of choice- and reward- selective neurons increases with uncertainty in OFC, but not in M2

Following analyses on each neuron's activity in predicting individual epochs of interest, we removed an increasing number of cells with the largest beta coefficients (**Supplementary Figure 3**). As expected, decoder accuracy steadily dropped as more neurons with large beta coefficients were removed. We show heatmap plots of average trial activity for neurons that were significantly selective (p<0.05) for *Chosen Side*, *Trial Outcome*, and *Reward Retrieval* (**Figure 3A-C**), as well as trial-by-trial raster plots of calcium activity from individual cells (**Figure 3G-I**)

M2 contained a higher ratio of neurons selective for *Chosen Side* than OFC throughout all schedules (GLM, β_{Area} = -0.238, p < 0.01). There was a significant interaction between area and schedule (GLM, $\beta_{AreaxSchedule}$ = 0.063, p = 0.007) (**Table 8**), reflecting the fact that the ratio of choice-selective neurons increased in OFC with uncertainty (GLM, $\beta_{Schedule}$ = 0.06, p < 0.01, **Figure 3D**), but was not influenced by uncertainty in M2 (GLM, $\beta_{Schedule}$ = 0.004, p = 0.78) (**Table 9**). Session (i.e., experience) was not a significant predictor of cell selectivity. Thus, the ratio of choice-selective neurons increases in OFC with uncertainty, but does not change with uncertainty in M2.

For the *Trial Outcome* epoch, we found a significant difference in the ratio of outcome-selective cells, with M2 once again containing a higher ratio than OFC (GLM, β_{Area} = -0.14, p = 0.01). This ratio was also not modulated by experience alone as session was not a significant predictor. There was a significant interaction of area and schedule (GLM, $\beta_{AreaxSchedule}$ = 0.05, p = 0.01, **Table 10**), resulting from the fact that the ratio of outcome-predictive neurons in M2

177 decreased with increasing reward uncertainty (GLM, $\beta_{Schedule}$ = 0.05, p = 0.04; **Figure 3E**),
178 whereas the ratio of outcome-predictive neurons in OFC was similar regardless of reward
179 uncertainty (GLM, $\beta_{Schedule}$ = 0.02, p = 0.15) (**Table 11**). Since uncertain outcomes are less
180 predictable, it is expected that the proportion of outcome-predictive neurons should decrease with
181 increasing reward uncertainty, as observed in M2. However, it is somewhat paradoxical to
182 observe that the proportion of neurons encoding reward outcome in OFC remains stable despite
183 decreases in the certainty of reward. One possible explanation for this could be that under
184 conditions of greater uncertainty, additional OFC neurons are recruited not only to encode
185 behavioral choices (as shown above) but also to encode reward outcome. If so, then this
186 recruitment of additional reward-selective neurons may counteract the decreased proportion of
187 such neurons that would otherwise result from increased uncertainty (as seen in M2).

188 Prior evidence suggests that value integration may occur at the time of *Reward Retrieval*
189 [27, 38-40], so we performed an additional analysis to measure the proportion of neurons that
190 were reward-selective during a 1-s time window centered on head entry into the reward port during
191 rewarded trials versus a corresponding time window from unrewarded trials (see Methods). There
192 was a larger percentage of reward-selective cells in M2 compared to OFC (GLM, β_{Area} = -0.27, p
193 = 0.02) with a significant Area by Schedule interaction (GLM, $\beta_{AreaXSchedule}$ = 0.1, p = 0.03) (**Table**
194 **12**), resulting from the fact that OFC exhibited a higher proportion of reward-selective neurons for
195 schedules with greater uncertainty (GLM, $\beta_{Schedule}$ = 0.09, p = 0.026, **Figure 3F**), whereas M2
196 showed a similar percentage of reward-selective neurons across all schedules (GLM, $\beta_{Schedule}$ = -
197 0.01, p = 0.44). Again, it is an increase in uncertainty and not experience (**Table 13**) that drives
198 this increase in the ratio of reward-selective cells in OFC, since session was once again not a
199 predictor of cell selectivity.

200

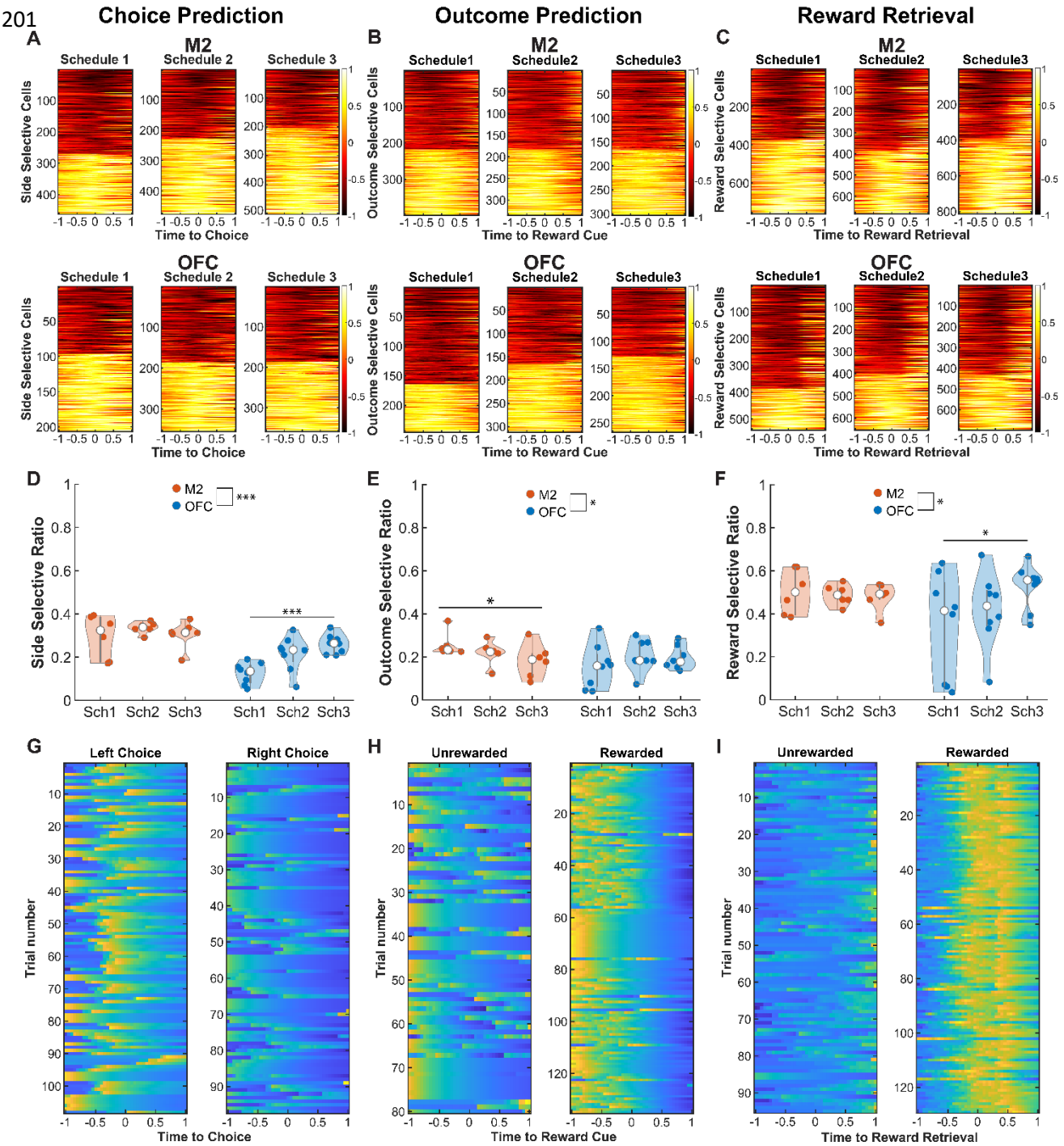

Figure 3. Decoder results are explained by changes in the ratio of selective cells across schedules. **(A)** Difference in trial averaged activity of left trials minus right trials at the time of choice. Cells plotted are neurons that had a significant effect of side in their activity and they are sorted from most negative beta coefficient to most positive one. Window is centered at choice. The activity of the neurons has been range-normalized. **(B)** Same as A but the difference is averaged activity of unrewarded trials minus rewarded trials. Window is centered at reward cue. **(C)** Same as A but the difference is averaged activity of unrewarded trials minus rewarded trials. Window is centered at reward retrieval. **(D)** Ratio of side selective neurons is overall larger in M2 but it increases with schedule only in OFC. **(E)** Ratio of outcome selective neurons is overall larger in M2 and decreases with uncertainty only in M2. **(F)** Ratio of reward selective neurons is overall larger in M2 but increases with schedule only in OFC. **(G)** Example of the z-score normalized activity of a significant side-selective neuron on left and right trials. **(H)** Same as G but for a significant outcome-selective cell. **(I)** Same as G but for a significant reward-selective neuron. ***p<0.001, *p=0.05.

202 **Behavioral strategies predict decoding accuracy in OFC, not in M2**

203 To assess the degree to which different behavioral measures (**Figure 4A-F**) modulated
204 decoding accuracy in OFC and M2, we analyzed the data using an omnibus mixed-effects GLM
205 for *Chosen Side* (**Table 14**) and *Trial Outcome* (**Table 16**). As predictors, we included primary
206 behavioral measures described above such as median initiation, choice, and reward latencies for
207 the entire session (**Figure 4I-K**), as well as secondary measures such as Win-Stay (WS,
208 proportion of trials when the rat repeated a response for which it had been rewarded on the
209 previous trial) and Lose-Shift (LS, proportion of trials when the rat did not repeat a response for
210 which it had been unrewarded on the previous trial), which we and others have previously used
211 to assess adaptive strategies in both stimulus and action-based learning [25, 41]. As other
212 predictors, we included a Flexibility Index (see Methods) that measured the animal's ability to
213 adapt to trial block reversals, and a Perseveration Index, or the mean number of trials to shift
214 choice behavior after being unrewarded, divided by the number of first unrewarded trials [42].

215 We found significant M2 vs. OFC area interaction effects for Win-Stay, Lose-Shift, and
216 Perseveration Index in the bin just before the choice epoch (**Figure 4H**, **Table 14**). Post-hoc
217 GLMs revealed that only initiation latencies (GLM: $\beta_{InitiationLatency} = -0.067$, $p = 0.0324$) significantly
218 predicted *Chosen Side* decoder accuracy for M2 (**Figure 4I**, **Table 15**). In contrast, WS (GLM:
219 $\beta_{WinStay} = 0.843$, $p = 0.0008$) and LS (GLM: $\beta_{LoseShift} = 1.466$, $p = 0.0240$) positively predicted,
220 whereas Perseveration Index (GLM: $\beta_{Perserveration\ Index} = -4.128$, $p < 0.0001$) negatively predicted
221 *Chosen Side* decoder accuracy in OFC (**Figure 4J**, **Table 19**). Similar post-hoc GLMs (**Figure**
222 **4K**, **Table 16**) found no significant behavioral predictors for *Trial Outcome* decoding accuracy in
223 M2 (**Figure 4L, Table 17**), but again found that WS (GLM: $\beta_{WinStay} = 0.652$, $p = 0.0202$) and LS
224 (GLM: $\beta_{LoseShift} = 1.550$, $p = 0.0228$) positively predicted and Perseveration Index (GLM: $\beta_{Perserveration}$
225 $_{Index} = -1.543$, $p = 0.0498$) negatively predicted *Trial Outcome* decoding accuracy in OFC (**Figure**
226 **4M, Table 21**). These analyses indicate that complex, strategy-level behaviors contribute to
227 decoding accuracy in OFC, but not M2.

228

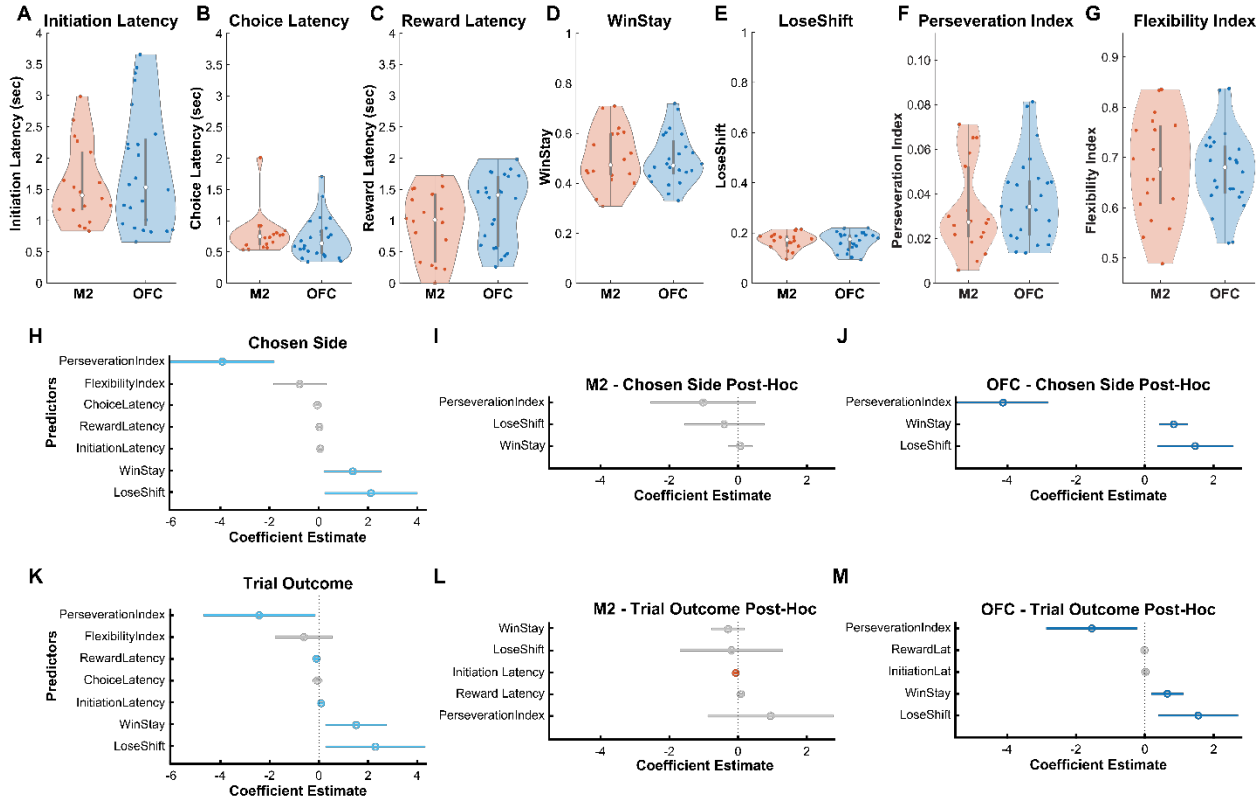

Figure 4. Chosen Side and Trial Outcome decoding accuracy is predicted by behavioral strategy only in OFC. **(A-G)** Behavioral measurements that were entered as regressors in omnibus Generalized Linear Models (GLM). Latency measures **(A-C)** were calculated as medians of all trials for each session. WinStay and LoseShift **(D-E)** were calculated as the proportion of total trials that were WinStay and LoseShift at the session level. Perserveration Index and Flexibility Index **(F-G)** were calculated using formulas described in the Methods. **(H)** Beta coefficients for regressors where significant area (M2 vs. OFC) interactions were found in predicting decoder accuracy of *Chosen Side*. Modeling was performed only on the accuracy from the bin right before choice (highlighted in yellow, Figure 2) **(I)** Post-Hoc GLM performed on sessions from rats with lenses in M2. **(J)** Post-Hoc GLM performed on sessions from rats with lenses in OFC. Strategy indices were significant predictors of *Chosen Side* decoding accuracy in OFC, but not in M2. **(K)** Beta coefficients for regressors where significant area (M2 vs. OFC) interactions were found in predicting *Trial Outcome*. Similarly, to H, analyses were only performed on the bin before reward cue (highlighted in yellow, Figure 2). **(L)** Post-Hoc GLM performed on sessions from rats with lenses in M2. **(M)** Post-Hoc GLM performed on sessions from rats with lenses in OFC. Strategy indices were significant predictors of *Trial Outcome* decoding accuracy in OFC, but not in M2.

DISCUSSION

We imaged single-cell activity in M2 and OFC while freely-moving rats underwent learning. Using a binary support vector machine decoder, we found evidence of functional heterogeneity in frontal cortex at both the population- and single-cell level. Specifically, M2 consistently contained more information about choice on individual trials than OFC, yet decoder accuracy increased with uncertainty, not just experience, only in OFC, not M2. We found that decoder accuracy was predicted by adaptive strategies in OFC, but not M2. We also determined that M2 and OFC

neurons exhibited different neural trajectories in learning trial types: these changed dynamically in more uncertain schedules in OFC, but not M2 (**Supplementary Figure 4**). Finally, our single cell analyses revealed a recruitment of an increasing ratio of choice- and reward- selective neurons in OFC with uncertainty, not M2. Collectively, these results suggest that neurons in OFC are more engaged in conditions with higher task demands that require adaptive strategies, such as increased uncertainty during learning.

There are several novel and confirmatory findings here. First, studies of neural activity in the frontal cortex in mice [43], rats [44, 45], and especially non-human primate subjects [46] typically involve extensive training prior to surgery to ensure that the animal is a task expert prior to any recording or imaging. In contrast, in the present experiment, rats learned the task *de novo* while we imaged single cells from these regions, which allowed us to determine that the dynamics in OFC changed as the uncertainty increased. Quite differently, M2 signaling of choice was robust and stable throughout the experiment. With the exception of two single-unit electrophysiological studies [11, 12], these two brain regions have not been systematically compared for their signaling in a reward-motivated task until now, and importantly, the previous studies administered a dynamic foraging task where subjects were not required to learn any task structure. We used a similar task to that in a recent report by Hattori and colleagues [37], but those authors also did not vary the uncertainty in the reward environment, as we did here. Consistent with their findings, we confirm that OFC plasticity is required for 'across session' learning (what authors call "meta-learning"), and here we extend this to conditions of increasing uncertainty encoded in OFC, but not in M2, neurons.

Studies following manipulations in rat OFC in flexible reward learning have included targeting the entire ventral surface [47, 48] or comparisons of medial vs. lateral OFC [23, 24]. Similar to a recent study using identical targeting [25], here we examined the role of ventrolateral OFC, a subregion not as often probed as medial and more lateral OFC [49], and found evidence consistent with its encoding of expected uncertainty [26]. Specifically, several studies using different methods [30-32, 50] suggest OFC must be 'online' to establish a baseline risk associated with probabilistic outcomes from which to gauge meaningful changes (i.e., reversals or block switches). OFC-inhibited animals also do not employ effective Win-Stay strategies [25], consistent with the GLM modeling results of the present experiment.

Here we find evidence that OFC neurons learn task structure details that are ultimately useful in predicting the consequences of decisions in uncertain and/or novel conditions [51]. In support of this, we found that OFC neurons do not encode choices as well during more certain

schedules, evidenced in both decoder and stability analyses where M2 decoder accuracy is greater than that of OFC in the more certain schedules. Additionally, we observed an increase in the proportion of neurons that signaled reward with increasing uncertainty in OFC, not in M2. These findings are consistent with the idea that OFC has a pivotal role in creating a task map [52, 53]: just as a spatial map helps one move better through space, a task map would help with adaptive behavioral strategies. We show evidence of this with decoder performance in OFC positively predicted by adaptive strategies WinStay, LoseShift, and negatively correlated with an inflexibility measure like Perseveration Index.

By comparison to OFC, M2 is often overlooked in learning studies due to its presumed stronger role in motor skill and action execution in both rodents and non-human primates [54-56]. There is evidence that M2 encodes task-relevant features, such as whether a rat will choose the left or right side in a bandit task [12] and a risky or safe option [57]. Thus, our results provide additional evidence that M2 encodes important task parameters such as choice and trial outcome. Even with recruitment of a decreasing proportion of outcome-selective cells with uncertainty (**Figure 3E**), this change ultimately had not impact on decoding accuracy of trial outcome in M2. Indeed, M2 is relatively unchanging: its encoding of choice remained robust and stable throughout schedules, and dynamics in this region contained a "full picture" of task-relevant features even from the initial phases of learning. Given that M2 biases decision-making processes [5, 10], an early read-out of “intention” could be a useful brain-machine interface application, given its stable coding through uncertainty.

These findings demonstrate distinct roles for M2 and OFC in processing task-specific information during learning under uncertainty, with M2 neurons maintaining robust, stable activity throughout learning, and OFC neurons exhibiting significant adaptations in response to uncertainty. This suggests a mechanism by which OFC neurons make adjustments to dynamic environments, while M2 provides a more consistent response control mechanism. Interestingly, unlike the present findings that suggest a role for rodent OFC in both outcome and reward probability encoding, primate OFC is not as important for encoding of reward “availability, as indexed by its probability” [58]. Instead, OFC is more specialized in primates for value and “desirability,” not probability. This may be an important primate-rodent difference to consider when interpreting experimental findings in frontal cortex across species in the future.

Acknowledgements

This work was supported by NIH 2R01DA047870, NSF NeuroNex 1707408, and F31MH135698. We thank the members of the Izquierdo and Wikenheiser labs for their feedback and suggestions. We would also like to thank the members of Romero Sosa's dissertation committee, Drs. Kate Wassum and Dean Buonomano, for their feedback on experimental design. Finally, we thank Dr. Dmitriy Lisitsyn for help setting up the CaImAn pipeline and Dr. Alireza Soltani for his valuable feedback on analyses and interpretation.

Author Contributions

AI: Conceptualization, methodology, formal analysis, data curation, resources, writing-original draft, writing- review & editing, software, visualization, supervision, and funding. **AW**: review & editing. **TB**: formal analysis, review & editing, supervision, funding. **JLRS**: Conceptualization, methodology, investigation & data collection, formal analysis, investigation, data curation, writing- original draft preparation, writing- review & editing, software, visualization, and funding.

METHODS

Subjects

Subjects for single-cell calcium imaging were N=7 adult Long-Evans rats: n=4 (3 males, 1 female) in OFC and n=3 (2 females, 1 male) in M2. Rats were obtained from a colony of GAD-Cre transgenic rats (RRRC#751; Rat Resource and Research Center, MO) / TH-Cre (RRRC#659; Rat Resource and Research Center, MO), genotyped as wildtype. Rats were pair-housed when they arrived at our housing facilities and then single-housed after undergoing surgery. Rats were housed in plastic transparent tubs filled with bedding media made of wood shavings in a room with a reverse 12-hour light cycle. Pretraining and testing occurred during their dark period, seven days per week until all experimental sessions were completed. Motivation was achieved through a progressive food restriction until the weight was kept above 85% of their initial free-feeding weight. Rats had free access to water at all times. Before training, rats were handled for 10-20 min for a minimum of 5 consecutive days. Subsequently, rats were introduced to a three-finger hold that enabled the plugging of a miniscope after surgery (usually 3-5 days). Experiments were conducted under the approval and following the guidelines established by the Chancellor's Animal Research Committee at UCLA.

Behavioral Pretraining

Our operant chambers were outfitted with a touchscreen on one end, divided into three zones (left, center, and right), and a reward port opposing the touchscreen (Lafeyette Instrument, Inc.). Ten sucrose pellets were placed in the rat's homecage one day before training to acclimate them to the pellets. The rats were placed in the operant chambers on the first training day, and ten pellets were dispensed. The rats remained in the chambers for 20 min, where they could explore, eat the pellets, and become habituated to the testing environment. The criterion for the rat to move on to the next phase is eating all ten pellets within the allotted time. The following day, they begin Initial Touch Center (ITC), which was the first time the rat had learned to interact with the touchscreen. A trial commenced with the display of a white rectangle in the center zone to indicate the rat is required to interact with it (e.g., nose poke or paw touch). Once the rat interacted with the center zone, a pellet was immediately delivered to the reward port. The rat only had 40-s to interact with the center zone before the rectangle disappeared, and the trial was counted as an initiation omission. If the rat successfully interacted with the center zone and collected the sucrose pellet, the trial was considered a committed trial. For the rat to move on from ITC, it had to complete 60 committed trials within 45 min. The final phase of pretraining was Immediate Reward (IR). In this phase, the rat was required to initiate the trial by touching the center zone when the white rectangle is presented, and then it was required to touch a stimulus presented pseudo randomly either on the left or right zone of the touchscreen. The rat had 60-s to interact with this stimulus to obtain a reward. Similar to the ITC criterion, for the rat to complete IR, it had to complete 60 committed trials within 45 minutes. After completing IR, rats were considered ready for surgery.

Miniscope Assembly

We purchased assembled Miniscope V4.4 kits from *Open Ephys*. The miniscope was placed in a 3D-printed, custom-designed, and constructed helmet (a link to the 3D design would be excellent here). The 3D-printed helmet enabled us to utilize a more resilient SMA connector for rat movement. Once the miniscope was fitted inside the helmet, we ensured LED power, the electrowetting lens, and the CMOS were working correctly. The tether used to connect the miniscope to the operating system had a female SMA connector on one end and a male HDMI connector on the opposite end. A motorized commutator from Doric Lenses (Part Number: AERJ_24_HDMI+4) allowed the tether to rotate with the rat. The commutator transferred the signal to the miniscope DAQ v3.3, also obtained from *Open Ephys*. The DAQ sent the signal over USB to a recording computer. Additionally, the DAQ produced a TTL pulse every time the

365 miniscope recorded a frame of data. These TTL pulses were recorded in parallel with TTL pulses
366 sent by the operant chamber whenever certain behaviors within a trial were performed (i.e., trial
367 initiation, reward port entry) and were used to time lock neural data to specific epochs within trials
368 and within single sessions. These TTL pulses were recorded using a CerePlex Direct data
369 acquisition system and later used to sync the neural data. The USB signal from the miniscope
370 was recorded onto a Framework Laptop 13 (11th Gen Intel) using the Miniscope DAQ Software
371 (build v1_11).

372 **GCaMP and Lens Implant Surgeries**

373 Rats were anesthetized with isoflurane (5% induction, 2% maintenance in 2.5 L/min O_2).
374 After clearing the skull, we leveled the skull by ensuring the difference in DV around Bregma was
375 not greater than 0.05 mm. An etchant was applied to the skull for 1 minute to ensure the adhesive
376 would adhere. After cleaning the etchant, we partially drilled seven tiny holes that would be used
377 for seven anchor screws (Fine Science Tools #19010-00). Two anchor screws were placed in the
378 very front, two directly posterior from Bregma, two anterior to Lambda, and one contralateral to
379 where the GRIN lens would be placed. Subsequently, a 1.2 mm diameter craniotomy was drilled
380 above the brain regions of interest. For OFC placement, the coordinates were AP: +3.7mm, ML:
381 +2.5mm, and for M2 placement, the coordinates were AP: +2.0mm, ML: +0.7mm. The craniotomy
382 was cleaned to ensure that the superior sagittal sinus was intact, and then the dura was carefully
383 removed. A 1uL Hamilton and Hamilton Pump (Part number) delivered GCaMP6f (Addgene, #
384 100834) through cannulae and injectors in either OFC or M2. For OFC surgeries, we unilaterally
385 infused virus into two different sites: AP: +3.7mm, ML: +2.5mm, DV: -4.6mm and AP: +3.7mm,
386 ML: +2.5mm, DV: -4.2mm. For M2, we also infused unilaterally into two different sites: AP:
387 +2.0mm, ML: +0.7mm, DV: -0.9mm and AP: +2.0mm, ML: +0.7mm, DV: -1.4mm. We dialed down
388 0.5mm more ventrally in either region to create a pocket for infusions. We then injected 0.5uL of
389 GCaMP6f per site, thus totaling 1uL of virus per surgery. The syringe was placed in a Hamilton
390 pump with a speed of 0.1uL per minute. After viral infusions, lens implantation occurred
391 immediately afterward. A 23-gauge needle was attached to the stereotax, zeroed at Bregma, and
392 then lowered to make clear a path for the lens. Next, the lens was lowered to the halfway point
393 between the DV coordinates as above using a vacuum. After the GRIN (Gradient Index) lens had
394 been placed in its location, we used viscous Loctite super glue to glue the sides of the lens to the
395 top of a dry skull, then added a layer of Metabond bone cement that coats the lens, anchor screws,
396 and the most superficial layer of the skull. After allowing 5-10 min for the Metabond to dry, we
397 poured opaque dental dement on the Metabond to fully cover the anchor screws and cover the

398 sides of (but not obscure) the GRIN lens. Before the dental cement thoroughly dried, we affixed
399 a custom 3D-printed lens cover. After drying the dental cement, we applied a layer of topical
400 antibiotic to the edge of the dental cement head cap.

401 We waited 3 to 4 weeks post-surgery to allow for GCaMP expression before attaching the
402 baseplate. We anesthetized the rat for baseplating, removed the lens protector, and cleaned the
403 top of the dental cement head cap. We attached a baseplate to a fully assembled miniscope using
404 a custom 3D holder. We lowered the miniscope and the baseplate until we could focus entirely
405 on the top of the implanted GRIN lens, searching for visible expression in the area of interest,
406 then fixing the baseplate using dental cement. GCaMP expression and lens implant
407 reconstructions are shown for OFC (**Figure 1D, left**) and for M2 (**Figure 1D, right**), along with
408 representative photomicrographs (**Figure 1E-F**)**.** All GCaMP and lens placements for all animals
409 are shown in **Supplementary Figure 1**.

410 **Behavioral Testing**

411 After the baseplating surgery, rats were again put on food restriction before behavioral
412 testing: they were eased into a restricted diet over three days to no more than 85% of their free-
413 feeding weight. Additionally, rats were once again habituated to a gentle hold and plugging the
414 miniscope into the baseplate. Rats were given a second round of pretraining as a sample imaging
415 session using a miniscope. We ensured rats performed many trials in the IR phase (> 200 trials
416 in 45 mins) before moving the rat onto the main behavioral task.

417 *Restless Bandit.* Similar to pretraining, a trial in the "restless bandit task" began when a
418 circle was displayed in the center zone of the touchscreen. The rat must interact with it by nose-
419 poking or touching it with its paw within 40-s; otherwise, it is scored as an initiation omission. After
420 touching the circle, two identical stimuli were presented on both the right and left touchscreen
421 zones. The rat had to interact with either the left or the right zones. The rat had 60-s to make a
422 choice otherwise, it was scored as a choice omission. One of the zones was associated with a
423 higher probability of reward, while the other was associated with a lower probability of reward. If
424 the rat received a sucrose pellet reward, it was dispensed in the reward port on the opposite side
425 of the chamber, and the subsequent trial began after a 10-s inter-trial interval (ITI). If the rat did
426 not receive a reward, a 5-s time-out was imposed in addition to the 10-s ITI. If the rat initiated a
427 trial and made a choice within the allotted time, the trial was scored as a committed trial regardless
428 of whether it was rewarded. Food motivation was assessed purely by the number of committed
429 trials, not accuracy. In each session, there were three blocks of 75 committed trials each.

From one block to the next, the location of the highest-valued side reversed. The probability of reward for each option varied depending on the session. There was an increase in uncertainty over testing. Task structure is visualized in **Figure 1A**. Violin plots for all initiation, choice, and reward latencies are shown by schedule (**Figure 1I-K**), and the median per session collapsed across all schedules (**Figure 3A-C**) for each of these groups.

Post-processing calcium imaging pipeline

Miniscope recording videos were processed using custom Python code and the Python version of CaImAn [59]. We concatenated videos and cropped them to focus the field of view (FOV) with the neural activity. We then passed it through the motion correction algorithm in CaImAn, with the central parameter *gSif_filt* set between 6 and 12 for our data. All of the motion correction for our data was conducted with the piece-wise rigid motion correction Boolean setting set to true. We performed the non-rigid algorithm if this algorithm did not fix the motion artifacts. Once the motion correction was completed, the motion-corrected videos were passed on to the CNMF-E portion of CaImAn [59]. The main parameters we used for the CNMF-E were as follows: the half size of a neuron = 8; the half size of the neuron's bounding box = 16; for every session, we chose a value to separate the first and most significant population of minimum peak-to-noise (PNR) ratio resulting in use of a range between 7-16; for the minimum correlation value we found values between 0.75 and 0.85 worked best. Every other setting was left to CaImAn default. After CNMF-E, we performed a component analysis. We set the Boolean parameter *use_cnn* to true so that CaImAn would use a trained convolution-neural network (CNN) model to assign a value between 0-1 that determined how close the components matched the appearance of soma. The algorithm used three different values to determine if a component should be as accepted as a cell: Spatial footprint consistency (*rval*), Signal-to-Noise ratio (*snr*), and CNN threshold value (*cnn_thr*), with the minimum values for each of these set to 2.5, 0.85, and 0.85, respectively. We then visually-inspected random components. Since, according to CaImAn documentation, it is not advised to calculate deltaF/F when using 1P data (due to the inability to confidently calculate baseline with background activity) we used the function *estimates.detrend_df_f* with the flag *detrend_only* set to true to calculate fluorescence where baseline has been subtracted but has not been normalized by it. Additional settings used were: quantileMin = 8, frames_window = 250, use_residuals = True. Finally, we calculated the deconvolved traces of the accepted components using the CaImAn function *estimates.deconvolve*. This removed any change in the fluorescence not due to the dynamics of the neurons. After the detrended and deconvolved values were calculated, all of the outputs were saved into a .mat file (MATLAB, MathWorks Inc., Natick, MA),

463 for all further processing. In MATLAB, we combined the output from CaImAn with TTL pulses to
464 align activity of neurons around specific epochs of behavior.

465 Some of the videos had banding artefact caused by a known issue with the USB controller
466 of the UCLA miniscope DAQ. When banding occurred, we first saved the frames in which this
467 occurred and then filled the frames with the last reliable frame before the banding. Following
468 processing with CaImAn, we replaced the data from those frames with NaNs.

469 **Data Analysis**

470 All data analyses were conducted using custom-written code in MATLAB.

471 *Learning and Performance.* The probability of choosing the better option was the primary
472 measure of interest, and secondarily Initiation Latency, Choice Latency, and Reward Latency
473 were each analyzed with a series of mixed-effects General Linear Models (GLMs) (*fitglme*
474 function; Statistics and Machine Learning Toolbox) first with omnibus analyses that included lens
475 group (M2-implanted, OFC-implanted). Follow-up GLMs were conducted pending significant
476 interactions in the omnibus models. All post-hoc tests were corrected for the number of
477 comparisons, with Holm correction. The coding of variables for GLM were: 0=females, 1=males,
478 0=OFC-implanted, and 1=M2-implanted). Statistical significance for GLM analyses was noted as
479 p-values of less than 0.05.

480 *Cross Validated Peak-Aligned Heatmap*. A window of detrended fluorescence 1 s before
481 and 3 s after choice was obtained for every trial in a session. This resulted in a matrix of cell-by-
482 frame-by-trial averaged across all trials for a resulting cell-by-frame matrix. This was normalized
483 using the normalize function on Matlab with the 'range' parameter. The max in a cell's activity was
484 1, and the minimum was 0 to ensure fair comparison across all cells in that session. The odd trials
485 of neurons were then peak aligned and the resulting indices were used to plot the even trials
486 using *imagesc*. Vertical dashed bars show the moment of choice and the moment of reward cue.

487 *Decoder Analysis*. A 4-s window of detrended fluorescence centered around Initiation was
488 obtained for every trial in a session. Separately, another 4-s window (1-s before and 3-s after) of
489 detrended fluorescence around choice was obtained for every trial in a session. This resulted in
490 a cell-by-frame-by-trial matrix for initiation and a separate one for choice. We temporally
491 downsampled so that activity in bin 1 was the average of frames 1-6, activity in bin 2 was the
492 average of frames 3-9, and so on. Every trial was also labeled as either a left or right choice,
493 whether rewarded or unrewarded (win or lose). One trial was left out for testing the decoder, and

494 the rest of the trials were then balanced so that there would be the same number of left-rewarded,
495 left-unrewarded, right-rewarded, and right-unrewarded conditions across all sessions in training
496 of the decoder. The balanced trials were randomly selected for every test trial to sample the entire
497 dataset of trials per session. Once the balanced subset of trials was selected, the neural data for
498 that session and the labels were inputted into the Matlab function *fitcsvm* with the
499 "KernelFunction" set to 'linear.' The decoder was then tested on the neural data for the test trial,
500 and the result was tallied as a 1 if the label matched the test label and a 0 if it was mismatched.
501 This was conducted for every single trial in a session. Additionally, we reran the decoder on all
502 trials per session, but with the trial type labels randomly shifted. This data is shown as "Shuffled"
503 in **Figure 2F-G**. Statistical comparisons and post-hocs were performed using Matlab's *fitglme*
504 function, and the formulas are included in the corresponding tables. Accuracy measures from the
505 bin (average of 5 frames) before choice were utilized for the *Chosen Side* GLMs and accuracy
506 measures before the reward cue were used for the *Trial Outcome* GLM.

507 *Single Cell Selectivity GLM*. Activity for every neuron was obtained on the same bins used
508 for the GLMs for decoder accuracy. In addition to *Chosen Side* and *Trial Outcome* activity, we
509 used the averaged activity 5 frames before and after *Reward Retrieval* for single cell selectivity
510 analysis. Statistics were conducted using Matlab's *fitglme* and the formulas for γ = neural activity
511 were γ ~ [1 + side] for Chosen Side and γ ~ [1 + rewarded] for both Trial Outcome and Reward
512 Retrieval. After a GLM was fitted for every cell per session, the ratio of selective cells (ones with
513 a p-value lower than 0.05) was obtained. We then fit GLM models to the ratios across both areas
514 and all three schedules.

515 *Behavioral measurements*. Latencies were recorded from ABET in Lafayette Instrument
516 chambers. Initiation latency measured the time from the presentation of the white circle on the
517 center touch zone until a rat interacts with the middle zone. Choice latency measured the time
518 from the presentation of both stimuli to the time the rat interacts with one of the stimuli to make a
519 choice. Reward latency measures the time from the dispensed pellet until the rat enters the reward
520 port to retrieve the pellet. WinStay was calculated as the percentage of all trials when the rat
521 received a reward on the previous trial and chose the same side for the following trial. LoseShift
522 was calculated as the percentage of all trials when the rat did not receive a reward and chose a
523 different side for the subsequent trial. The Perseveration Index was calculated as the average
524 number of trials to change choice after being unrewarded. Flexibility Index was calculated as
525 follows:

526 $$FlexIndex = mean[(mean(C_{Better}\text{Block1}, C_{Better}\text{Block2}), (mean(C_{Better}\text{Block2}, C_{Better}\text{Block3})]$$

where C_{Better} is equal to 1 if the animal chose the better option and 0 otherwise, with the better option defined according to the reward schedule for each block. Statistical comparisons and post-hocs were performed using Matlab's *fitglme* function, and the formulas are included in the corresponding tables. Accuracy measures from the bin before choice were utilized for the *Chosen Side* GLMs and accuracy measures from the bin before the reward cue were used for the *Trial Outcome* GLM.

REFERENCES

1. Reep, R.L., G.S. Goodwin, and J.V. Corwin, *Topographic organization in the corticocortical connections of medial agranular cortex in rats.* J Comp Neurol, 1990. **294**(2): p. 262-80.
2. Reep, R.L. and J.V. Corwin, *Topographic organization of the striatal and thalamic connections of rat medial agranular cortex.* Brain Res, 1999. **841**(1-2): p. 43-52.
3. Gremel, C.M. and R.M. Costa, *Premotor cortex is critical for goal-directed actions.* Front Comput Neurosci, 2013. **7**: p. 110.
4. Barthas, F. and A.C. Kwan, *Secondary Motor Cortex: Where 'Sensory' Meets 'Motor' in the Rodent Frontal Cortex.* Trends Neurosci, 2017. **40**(3): p. 181-193.
5. Murakami, M., et al., *Neural antecedents of self-initiated actions in secondary motor cortex.* Nat Neurosci, 2014. **17**(11): p. 1574-82.
6. Ostlund, S.B., N.E. Winterbauer, and B.W. Balleine, *Evidence of action sequence chunking in goal-directed instrumental conditioning and its dependence on the dorsomedial prefrontal cortex.* J Neurosci, 2009. **29**(25): p. 8280-7.
7. Siniscalchi, M.J., et al., *Fast and slow transitions in frontal ensemble activity during flexible sensorimotor behavior.* Nature Neuroscience, 2016. **19**(9): p. 1234-1242.
8. Erlich, J.C., M. Bialek, and C.D. Brody, *A cortical substrate for memory-guided orienting in the rat.* Neuron, 2011. **72**(2): p. 330-43.
9. Ebbesen, C.L., et al., *More than Just a "Motor": Recent Surprises from the Frontal Cortex.* J Neurosci, 2018. **38**(44): p. 9402-9413.
10. Yang, J.H. and A.C. Kwan, *Secondary motor cortex: Broadcasting and biasing animal's decisions through long-range circuits.* Int Rev Neurobiol, 2021. **158**: p. 443-470.
11. Sul, J.H., et al., *Distinct roles of rodent orbitofrontal and medial prefrontal cortex in decision making.* Neuron, 2010. **66**(3): p. 449-60.
12. Sul, J.H., et al., *Role of rodent secondary motor cortex in value-based action selection.* Nat Neurosci, 2011. **14**(9): p. 1202-8.
13. Tsuchida, A., B.B. Doll, and L.K. Fellows, *Beyond reversal: a critical role for human orbitofrontal cortex in flexible learning from probabilistic feedback.* J Neurosci, 2010. **30**(50): p. 16868-75.
14. Gardner, M.P. and G. Schoenbaum, *The orbitofrontal cartographer.* Behavioral neuroscience, 2021. **135**(2): p. 267.
15. Rudebeck, P.H. and E.A. Murray, *The orbitofrontal oracle: cortical mechanisms for the prediction and evaluation of specific behavioral outcomes.* Neuron, 2014. **84**(6): p. 1143-56.
16. Izquierdo, A., et al., *The neural basis of reversal learning: An updated perspective.* Neuroscience, 2017. **345**: p. 12-26.
17. Zhou, J., et al., *Prospective representations in rat orbitofrontal ensembles.* Behav Neurosci, 2021. **135**(4): p. 518-527.
18. Campos, M., et al., *Orbitofrontal cortical activity during repeated free choice.* Journal of Neurophysiology, 2012. **107**(12): p. 3246-3255.

19. Kimmel, D.L., et al., *Value and choice as separable and stable representations in orbitofrontal cortex.* Nature Communications, 2020. **11**(1): p. 3466.
20. Luk, C.H. and J.D. Wallis, *Choice coding in frontal cortex during stimulus-guided or action-guided decision-making.* J Neurosci, 2013. **33**(5): p. 1864-71.
21. Feierstein, C.E., et al., *Representation of Spatial Goals in Rat Orbitofrontal Cortex.* Neuron, 2006. **51**(4): p. 495-507.
22. Dalton, G.L., et al., *Multifaceted Contributions by Different Regions of the Orbitofrontal and Medial Prefrontal Cortex to Probabilistic Reversal Learning.* J Neurosci, 2016. **36**(6): p. 1996-2006.
23. Hervig, M.E., et al., *Dissociable and Paradoxical Roles of Rat Medial and Lateral Orbitofrontal Cortex in Visual Serial Reversal Learning.* Cerebral Cortex, 2019. **30**(3): p. 1016-1029.
24. Verharen, J.P.H., et al., *Modulation of value-based decision making behavior by subregions of the rat prefrontal cortex.* Psychopharmacology, 2020. **237**(5): p. 1267-1280.
25. Aguirre, C.G., et al., *Dissociable Contributions of Basolateral Amygdala and Ventrolateral Orbitofrontal Cortex to Flexible Learning Under Uncertainty.* J Neurosci, 2024. **44**(2).
26. Soltani, A. and A. Izquierdo, *Adaptive learning under expected and unexpected uncertainty.* Nat Rev Neurosci, 2019. **20**(10): p. 635-644.
27. Young, J.J. and M.L. Shapiro, *The orbitofrontal cortex and response selection.* Ann N Y Acad Sci, 2011. **1239**: p. 25-32.
28. Keiflin, R., et al., *The orbitofrontal cortex as part of a hierarchical neural system mediating choice between two good options.* Journal of Neuroscience, 2013. **33**(40): p. 15989-15998.
29. Groman, S.M., et al., *Orbitofrontal Circuits Control Multiple Reinforcement-Learning Processes.* Neuron, 2019. **103**(4): p. 734-746 e3.
30. Namboodiri, V.M.K., et al., *Single-cell activity tracking reveals that orbitofrontal neurons acquire and maintain a long-term memory to guide behavioral adaptation.* Nat Neurosci, 2019. **22**(7): p. 1110-1121.
31. Jenni, N.L., G. Rutledge, and S.B. Floresco, *Distinct Medial Orbitofrontal-Striatal Circuits Support Dissociable Component Processes of Risk/Reward Decision-Making.* J Neurosci, 2022. **42**(13): p. 2743-2755.
32. Stolyarova, A. and A. Izquierdo, *Complementary contributions of basolateral amygdala and orbitofrontal cortex to value learning under uncertainty.* Elife, 2017. **6**.
33. Jo, S. and M.W. Jung, *Differential coding of uncertain reward in rat insular and orbitofrontal cortex.* Sci Rep, 2016. **6**: p. 24085.
34. Riceberg, J.S. and M.L. Shapiro, *Orbitofrontal cortex signals expected outcomes with predictive codes when stable contingencies promote the integration of reward history.* Journal of Neuroscience, 2017. **37**(8): p. 2010-2021.
35. O'Neill, M. and W. Schultz, *Coding of Reward Risk by Orbitofrontal Neurons Is Mostly Distinct from Coding of Reward Value.* Neuron, 2010. **68**(4): p. 789-800.
36. O'Neill, M. and W. Schultz, *Risk Prediction Error Coding in Orbitofrontal Neurons.* The Journal of Neuroscience, 2013. **33**(40): p. 15810-15814.
37. Hattori, R., et al., *Meta-reinforcement learning via orbitofrontal cortex.* Nat Neurosci, 2023. **26**(12): p. 2182-2191.
38. Izquierdo, A., R.K. Suda, and E.A. Murray, *Bilateral Orbital Prefrontal Cortex Lesions in Rhesus Monkeys Disrupt Choices Guided by Both Reward Value and Reward Contingency.* The Journal of Neuroscience, 2004. **24**(34): p. 7540-7548.
39. Ostlund, S.B. and B.W. Balleine, *Orbitofrontal Cortex Mediates Outcome Encoding in Pavlovian But Not Instrumental Conditioning.* The Journal of Neuroscience, 2007. **27**(18): p. 4819-4825.
40. Schoenbaum, G., et al., *A new perspective on the role of the orbitofrontal cortex in adaptive behaviour.* Nature Reviews Neuroscience, 2009. **10**(12): p. 885-892.

41. Harris, C., et al., *Unique features of stimulus-based probabilistic reversal learning.* Behav Neurosci, 2021. **135**(4): p. 550-570.
42. Brigman, J.L., et al., *Pharmacological or genetic inactivation of the serotonin transporter improves reversal learning in mice.* Cereb Cortex, 2010. **20**(8): p. 1955-63.
43. Bari, B.A., et al., *Stable Representations of Decision Variables for Flexible Behavior.* Neuron, 2019. **103**(5): p. 922-933.e7.
44. Hart, E.E., M.P.H. Gardner, and G. Schoenbaum, *Anterior cingulate neurons signal neutral cue pairings during sensory preconditioning.* Current Biology, 2022. **32**(3): p. 725-732.e3.
45. Constantinople, C.M., et al., *Lateral orbitofrontal cortex promotes trial-by-trial learning of risky, but not spatial, biases.* eLife, 2019. **8**: p. e49744.
46. Padoa-Schioppa, C. and J.A. Assad, *The representation of economic value in the orbitofrontal cortex is invariant for changes of menu.* Nature Neuroscience, 2008. **11**(1): p. 95-102.
47. Izquierdo, A., *Functional Heterogeneity within Rat Orbitofrontal Cortex in Reward Learning and Decision Making.* J Neurosci, 2017. **37**(44): p. 10529-10540.
48. Izquierdo, A., et al., *Basolateral amygdala lesions facilitate reward choices after negative feedback in rats.* J Neurosci, 2013. **33**(9): p. 4105-9.
49. Zimmermann, K.S., et al., *Memory Retention Involves the Ventrolateral Orbitofrontal Cortex: Comparison with the Basolateral Amygdala.* Neuropsychopharmacology, 2018. **43**(2): p. 373-383.
50. K Namboodiri, V.M., et al., *Relative salience signaling within a thalamo-orbitofrontal circuit governs learning rate.* Current Biology, 2021. **31**(23): p. 5176-5191.e5.
51. Rudebeck, Peter H. and Elisabeth A. Murray, *The Orbitofrontal Oracle: Cortical Mechanisms for the Prediction and Evaluation of Specific Behavioral Outcomes.* Neuron, 2014. **84**(6): p. 1143-1156.
52. Wikenheiser, A.M. and G. Schoenbaum, *Over the river, through the woods: cognitive maps in the hippocampus and orbitofrontal cortex.* Nat Rev Neurosci, 2016. **17**(8): p. 513-23.
53. Costa, K.M., et al., *The role of the lateral orbitofrontal cortex in creating cognitive maps.* Nat Neurosci, 2023. **26**(1): p. 107-115.
54. Alaverdashvili, M. and I.Q. Whishaw, *Motor cortex stroke impairs individual digit movement in skilled reaching by the rat.* European Journal of Neuroscience, 2008. **28**(2): p. 311-322.
55. LAWRENCE, D.G. and H.G.J.M. KUYPERS, *THE FUNCTIONAL ORGANIZATION OF THE MOTOR SYSTEM IN THE MONKEY1: I. THE EFFECTS OF BILATERAL PYRAMIDAL LESIONS.* Brain, 1968. **91**(1): p. 1-14.
56. Whishaw, I.Q., *Loss of the innate cortical engram for action patterns used in skilled reaching and the development of behavioral compensation following motor cortex lesions in the rat.* Neuropharmacology, 2000. **39**(5): p. 788-805.
57. Bao, C., et al., *The rat frontal orienting field dynamically encodes value for economic decisions under risk.* Nature Neuroscience, 2023. **26**(11): p. 1942-1952.
58. Rudebeck, P.H., et al., *Specialized Representations of Value in the Orbital and Ventrolateral Prefrontal Cortex: Desirability versus Availability of Outcomes.* Neuron, 2017. **95**(5): p. 1208-1220 e5.
59. Giovannucci, A., et al., *CaImAn an open source tool for scalable calcium imaging data analysis.* eLife, 2019. **8**: p. e38173.

TABLE 1

Across all Blocks in all Sessions for Rats with Lens Implants **γ = Percent Correct**							
Formula	γ~[1+Session*Block*TrialNum*Area+(1+Session*Block*TrialNum|RatID)]						
Coefficients	**β**	SE	tStat	DF	P	CIL	CIU
Intercept	0.8401	0.1821	4.6124	9434	<0.0001	0.4831	1.1971
TrialNumber	0.0066	0.0025	2.5965	9434	**0.0094**	0.0016	0.0115
Session	-0.0075	0.3257	-0.0230	9434	0.9817	-0.6459	0.6309
Area	-0.0724	0.2409	-0.3005	9434	0.7638	-0.5447	0.3999
Block	-0.4390	0.0876	-5.0140	9434	**<0.0001**	-0.6106	-0.2674
TrialNumber:Session	-0.0007	0.0027	-0.2641	9434	0.7917	-0.0060	0.0046
TrialNum:Implant	0.0044	0.0033	1.3035	9434	0.1924	-0.0022	0.0109
Session:Implant	0.0483	0.4308	0.1121	9434	0.9107	-0.7962	0.8928
TrialNum:Block	-0.0001	0.0020	-0.0543	9434	0.9567	-0.0041	0.0039
Session:Block	0.0488	0.0733	0.6657	9434	0.5056	-0.0949	0.1926
Implant:Block	-0.0773	0.1158	-0.6672	9434	0.5046	-0.3043	0.1498
TrialNum:Session:Implant	-0.0010	0.0036	-0.2744	9434	0.7838	-0.0080	0.0060
TrialNum:Session:Block	0.0000	0.0013	-0.0309	9434	0.9753	-0.0025	0.0025
TrialNum:Implant:Block	-0.0010	0.0027	-0.3801	9434	0.7039	-0.0063	0.0043
Session:Implant:Block	-0.0129	0.0970	-0.1331	9434	0.8941	-0.2031	0.1773
TrialNum:Session:Implant:Block	0.0003	0.0017	0.2017	9434	0.8401	-0.0030	0.0036

Alpha Level 0.05.

TABLE 2

Across all Blocks in all Sessions Comparing Lens Rats

γ = Initiation Latency

Formula	γ~[1+Session*Block*TrialNum+Implant+(1+Session*Block*TrialNum|RatID)]						
Coefficients	**β**	SE	tStat	DF	P	CIL	CIU
(Intercept)	5.7688	1.5593	3.6996	9441	0.0002	2.7123	8.8254
TrialNum	-0.0450	0.0147	-3.0611	9441	**0.0022**	-0.0737	-0.0162
Session	-0.2227	0.2056	-1.0833	9441	0.2787	-0.6257	0.1803
Implant_OFC	-0.4731	0.3832	-1.2344	9441	0.2171	-1.2242	0.2781
Block	0.0716	0.8186	0.0874	9441	0.9303	-1.5330	1.6762
TrialNum:Session	0.0053	0.0027	2.0071	9441	**0.0448**	0.0001	0.0105
TrialNum:Block	0.0114	0.0048	2.3661	9441	**0.0180**	0.0020	0.0209
Session:Block	-0.1536	0.1565	-0.9820	9441	0.3261	-0.4603	0.1530
TrialNum:Session:Block	-0.0010	0.0008	-1.2089	9441	0.2267	-0.0026	0.0006

Alpha Level 0.05

TABLE 3

Across all Blocks in all Sessions Comparing Lens Rats

γ = Choice Latency

Formula	γ~[1+Session*Block*TrialNum+Implant+(1+Session*Block*TrialNum|RatID)]						
Coefficients	**β**	SE	tStat	DF	P	CIL	CIU
(Intercept)	2.0249	0.6468	3.1304	9441	0.0018	0.7569	3.2928
TrialNum	-0.0085	0.0065	-1.3061	9441	0.1916	-0.0213	0.0043
Session	0.0307	0.2050	0.1498	9441	0.8810	-0.3712	0.4326
Implant_OFC	-0.5705	0.1600	-3.5666	9441	**0.0004**	-0.8840	-0.2569
Block	0.6944	0.4989	1.3920	9441	0.1640	-0.2835	1.6724
TrialNum:Session	-0.0006	0.0022	-0.2781	9441	0.7809	-0.0048	0.0036
TrialNum:Block	-0.0004	0.0032	-0.1219	9441	0.9030	-0.0066	0.0058
Session:Block	-0.1717	0.1449	-1.1843	9441	0.2363	-0.4558	0.1125
TrialNum:Session:Block	0.0008	0.0007	1.0717	9441	0.2839	-0.0006	0.0022

Alpha Leve 0.05.

TABLE 4

Across all Blocks in all Sessions Comparing Lens Rats

γ = Reward Latency

Formula	γ~[1+Session*Block*TrialNum+Implant+(1+Session*Block*TrialNum|RatID)]						
Coefficients	**β**	SE	tStat	DF	P	CIL	CIU
(Intercept)	1.5710	0.4575	3.4336	5809	0.0006	0.6740	2.4679
TrialNum	-0.0024	0.0032	-0.7300	5809	0.4654	-0.0087	0.0040
Session	-0.0524	0.0695	-0.7539	5809	0.4509	-0.1887	0.0839
Implant_OFC	-0.3749	0.2199	-1.7047	5809	0.0883	-0.8060	0.0562
Block	0.2466	0.2591	0.9518	5809	0.3413	-0.2613	0.7545
TrialNum:Session	0.0002	0.0005	0.4166	5809	0.6770	-0.0008	0.0012
TrialNum:Block	-0.0002	0.0017	-0.0989	5809	0.9212	-0.0036	0.0032
Session:Block	-0.0540	0.0441	-1.2253	5809	0.2205	-0.1405	0.0324
TrialNum:Session:Block	0.0001	0.0003	0.2610	5809	0.7941	-0.0005	0.0007

Alpha Level 0.05

TABLE 5

Comparing Chosen Side Decoder Accuracy Across all Schedules in M2 and OFC **γ = Decoder Accuracy before Choice**							
Formula	γ~[1+Area*Schedule+Session+(1|RatID:Session)]						
Coefficients	**β**	SE	tStat	DF	P	CIL	CIU
(Intercept)	1.0210	0.0983	10.389	37	<0.0001	0.8219	1.2202
Area	-0.2312	0.0593	-3.9013	37	**0.0004**	-0.3513	-0.1111
Session	0.0268	0.0222	1.2109	37	0.2336	-0.0181	0.0718
Schedule	-0.0843	0.0633	-1.3307	37	0.1914	-0.2126	0.0440
Area:Schedule	0.0562	0.0274	2.0500	37	**0.0475**	0.0007	0.1118

Alpha Level 0.05**.**

TABLES 6 (Table 5 Post-Hoc)

Comparing Chosen Side Decoder Accuracy Across Schedules 1 ONLY in M2 and OFC **γ = Decoder Accuracy before Choice in Schedule 1**							
Formula	γ~[1+Area+(1|RatID:Session)]						
Coefficients	**β**	SE	tStat	DF	P	CIL	CIU
(Intercept)	0.9752	0.0661	14.755	12	<0.0001	0.8312	1.1192
Area	-0.1746	0.0401	-4.3533	12	**0.0009**	-0.2620	-0.0872

Comparing Chosen Side Decoder Accuracy Across Schedules 2 ONLY in M2 and OFC **γ = Decoder Accuracy before Choice in Schedule 2**							
Formula	γ~[1+Area+(1|RatID:Session)]						
Coefficients	**β**	SE	tStat	DF	P	CIL	CIU
(Intercept)	0.9503	0.0747	12.7138	12	<0.0001	0.787	1.113
Area	-0.1195	0.0454	-2.6330	12	**0.0219**	-0.218	-0.021

Comparing Chosen Side Decoder Accuracy Across Schedules 3 ONLY in M2 and OFC **γ = Decoder Accuracy before Choice in Schedule 3**							
Formula	γ~[1+Area+(1|RatID:Session)]						
Coefficients	**β**	SE	tStat	DF	P	CIL	CIU
(Intercept)	0.9140	0.0522	17.5113	12	<0.0001	0.800	1.028
Area	-0.0621	0.0317	-1.9613	12	0.0735	-0.131	0.007

Alpha Level 0.05.

683 **TABLE 7**

Comparing Trial Outcome Decoder Accuracy Across all Schedules in M2 and OFC **γ = Decoder Accuracy before Reward Cue**							
Formula	γ~[1+Area*Schedule+Session+(1|RatID:Session)]						
Coefficients	**β**	SE	tStat	DF	P	CIL	CIU
(Intercept)	0.8561	0.0976	8.7707	37	<0.0001	0.6583	1.0539
Area	-0.1378	0.0589	-2.3405	37	**0.0248**	-0.2571	-0.0185
Session	0.0300	0.0220	1.3612	37	0.1817	-0.0146	0.0746
Schedule	-0.1278	0.0629	-2.0321	37	**0.0494**	-0.2552	-0.0004
Area:Schedule	0.0482	0.0273	1.7686	37	0.0852	-0.0070	0.1034

684 Alpha Level 0.05.

685

686

TABLE 8

Comparing the Ratio of Side Selective Neurons Across all schedules in M2 and OFC **γ = Ratio of Side Selective Neurons**							
Formula	γ~[1+Area*Schedule+Session+(1|RatID)]						
Coefficients	**β**	SE	tStat	DF	P	CIL	CIU
(Intercept)	0.5512	0.0824	6.6895	37	<0.0001	0.3843	0.7182
Session	0.0208	0.0179	1.1569	37	0.2547	-0.0156	0.0571
Schedule	-0.0999	0.0512	-1.9501	37	0.0588	-0.2037	0.0039
Area	-0.2375	0.0497	-4.7775	37	**<0.0001**	-0.3383	-0.1368
Area:Schedule	0.0630	0.0222	2.8364	37	**0.0074**	0.0180	0.1079

Alpha Level 0.05

TABLE 9 (Table 8 Post-Hoc)

Comparing the Ratio of Side Selective Neurons Across all Schedules in M2 ONLY **γ = Ratio of Side Selective Neurons in M2**							
Formula	γ~[1+Schedule+(1|RatID)]						
Coefficients	**β**	SE	tStat	DF	P	CIL	CIU
(Intercept)	0.3033	0.0407	7.4487	16	<0.0001	0.2170	0.3896
Schedule	0.0046	0.0166	0.2758	16	0.7862	-0.0305	0.0397
Comparing the Ratio of Side Selective Neurons Across all Schedules in OFC ONLY **γ = Ratio of Side Selective Neurons in OFC**							
Formula	γ~[1+Schedule+(1|RatID)]						
Coefficients	**β**	SE	tStat	DF	P	CIL	CIU
(Intercept)	0.0658	0.0310	2.1207	22	<0.0001	0.0015	0.1301
Schedule	0.0675	0.0144	4.7031	22	**0.0001**	0.0378	0.0973

Alpha Level 0.05.

TABLE 10

Comparing the Ratio of Outcome Selective Neurons Across all schedules in M2 and OFC **γ = Ratio of Outcome Selective Neurons**							
Formula	γ~[1+Area*Schedule+Session+(1|RatID)]						
Coefficients	**β**	SE	tStat	DF	P	CIL	CIU
(Intercept)	0.4403	0.0906	4.8611	37	<0.0001	0.2568	0.6238
Session	-0.0022	0.0173	-0.1268	37	0.8998	-0.0373	0.0329
Schedule	-0.0893	0.0495	-1.8025	37	0.0796	-0.1896	0.0111
Area	-0.1480	0.0547	-2.7053	37	**0.0103**	-0.2589	-0.0372
Area:Schedule	0.0567	0.0215	2.6416	37	**0.0120**	0.0132	0.1002

Alpha Level 0.05

TABLE 11 (Table 10 Post-Hoc)

Comparing the Ratio of Outcome Selective Neurons Across all Schedules in M2 ONLY **γ = Ratio of Outcome Selective Neurons in M2**							
Formula	γ~[1+Schedule+(1|RatID)]						
Coefficients	**β**	SE	tStat	DF	P	CIL	CIU
(Intercept)	0.2933	0.0365	8.0415	16	<0.0001	0.2160	0.3707
Schedule	-0.0370	0.0169	-2.1900	16	**0.0437**	-0.0728	-0.0012
Comparing the Ratio of Outcome Selective Neurons Across all Schedules in OFC ONLY **γ = Ratio of Outcome Selective Neurons in OFC**							
Formula	γ~[1+Schedule+(1|RatID)]						
Coefficients	**β**	SE	tStat	DF	P	CIL	CIU
(Intercept)	0.1453	0.0386	3.7607	22	0.0011	0.0652	0.2254
Schedule	0.0197	0.0133	1.4809	22	0.1528	-0.0079	0.0473

Alpha Level 0.05.

TABLE 12

Comparing the Ratio of Reward Selective Neurons Across all schedules in M2 and OFC **γ = Ratio of Reward Selective Neurons**							
Formula	γ~[1+Area*Schedule+Session+(1|RatID)]						
Coefficients	**β**	SE	tStat	DF	P	CIL	CIU
(Intercept)	0.7851	0.1869	4.2009	37	0.0002	0.4064	1.1638
Session	0.0018	0.0379	0.0487	37	0.9614	-0.0750	0.0787
Schedule	-0.1200	0.1083	-1.1076	37	0.2752	-0.3394	0.0995
Area	-0.2711	0.1129	-2.4018	37	**0.0215**	-0.4997	-0.0424
Area:Schedule	0.1047	0.0469	2.2316	37	**0.0318**	0.0096	0.1998

Alpha Level 0.05

TABLE 13 (Table 12 Post-Hoc)

Comparing the Ratio of Reward Selective Neurons Across all Schedules in M2 ONLY **γ = Ratio of Reward Selective Neurons in M2**							
Formula	γ~[1+Schedule+(1|RatID)]						
Coefficients	**β**	SE	tStat	DF	P	CIL	CIU
(Intercept)	0.5131	0.0421	12.2008	16	<0.0001	0.4240	0.6023
Schedule	-0.0115	0.0148	-0.7801	16	0.4467	-0.0429	0.0198
Comparing the Ratio of Reward Selective Neurons Across all Schedules in OFC ONLY **γ = Ratio of Reward Selective Neurons in OFC**							
Formula	γ~[1+Schedule+(1|RatID)]						
Coefficients	**β**	SE	tStat	DF	P	CIL	CIU
(Intercept)	0.2421	0.0925	2.6171	22	0.0157	0.0502	0.4339
Schedule	0.0932	0.0391	2.3833	22	**0.0262**	0.0121	0.1743

Alpha Level 0.05.

TABLE 14

Decoder Accuracy modeled by Behavioral Measurements.

γ = Chosen Side Decoder Accuracy

Formula	γ~[1+Session+FlexibilityIndex+PerserverationIndex+InitiationLatency+ChoiceLatency +RewardLatency+WinStay+LoseShift+Area*(Session+FlexibilityIndex+PerserverationIndex+InitiationLatency+ChoiceLatency+RewardLatency+WinStay+LoseShift)+(1|RatID:Session)]						
Coefficients	**β**	SE	tStat	DF	P	CIL	CIU
(Intercept)	1.2994	0.4269	3.0436	25	0.0054	0.4201	2.1787
Initiation Latency	-0.0739	0.0653	-1.1326	25	0.2681	-0.2083	0.0605
Choice Latency	0.0264	0.1127	0.2344	25	0.8166	-0.2057	0.2586
Reward Latency	-0.0873	0.0783	-1.1152	25	0.2754	-0.2484	0.0739
WinStay	-1.5011	0.8803	-1.7052	25	0.1006	-3.3140	0.3119
Area	-0.5611	0.2587	-2.1691	25	**0.0398**	-1.0939	-0.0283
LoseShift	-2.2113	1.4948	-1.4793	25	0.1515	-5.2899	0.8673
Flexibility Index	1.1537	0.8096	1.4250	25	0.1665	-0.5137	2.8211
Perseveration Index	3.9990	1.6714	2.3926	25	**0.0246**	0.5566	7.4413
Session	0.0035	0.0099	0.3565	25	0.7244	-0.0168	0.0238
Area:InitiationLatency	0.0608	0.0407	1.4962	25	0.1471	-0.0229	0.1446
Area:ChoiceLatency	-0.0599	0.0841	-0.7127	25	0.4826	-0.2331	0.1132
Area:RewardLatency	0.0242	0.0438	0.5542	25	0.5844	-0.0659	0.1144
Area:Win Stay	1.3807	0.5670	2.4352	25	**0.0224**	0.2130	2.5485
Area:Lose Shift	2.1181	0.9107	2.3258	25	**0.0284**	0.2425	3.9937
Area:Flexibility Index	-0.7755	0.5260	-1.4743	25	0.1529	-1.8589	0.3078
Area:Perseveration Index	-3.9170	1.0290	-3.8066	25	**0.0008**	-6.0363	-1.7978

Alpha Level 0.05

TABLE 15 (Table 14 Post-Hoc)

Post-Hoc Statistics on Area Interaction with M2 Lens Rats only **γ = Chosen Side Decoder Accuracy in M2 Rats**							
Formula	γ~[1+PerseverationIndex+WinStay+LoseShift+(1|RatID:Session)]						
Coefficients	**β**	SE	tStat	DF	P	CIL	CIU
(Intercept)	0.9846	0.1674	5.8818	14	<0.0001	0.6255	1.3436
Win Stay	-0.0131	0.1558	-0.0839	14	0.9343	-0.3472	0.3210
Lose Shift	-0.6778	0.5746	-1.1796	14	0.2578	-1.9102	0.5546
Perseveration Index	-1.0741	0.7841	-1.3699	14	0.1923	-2.7559	0.6076

Post-Hoc Statistics on Area Interaction with OFC Lens Rats only **γ = Chosen Side Decoder Accuracy in OFC Rats**							
Formula	γ~[1+PerseverationIndex+WinStay+LoseShift+(1|RatID:Session)]						
Coefficients	**β**	SE	tStat	DF	P	CIL	CIU
(Intercept)	0.2041	0.1828	1.1167	20	0.2774	-0.1771	0.5853
Win Stay	0.8435	0.2010	4.1975	20	**0.0004**	0.4243	1.2627
Lose Shift	1.4664	0.5304	2.7648	20	**0.0120**	0.3600	2.5729
Perseveration Index	-4.1286	0.6312	-6.5405	20	**<0.0001**	-5.4453	-2.8118

Alpha Level 0.05.

TABLE 16

Decoder Accuracy modeled by Behavioral Measurements.
γ = **Trial Outcome Decoder Accuracy**

Formula	γ~[1+Session+FlexibilityIndex+PerserverationIndex+InitiationLatency+ChoiceLatency+RewardLatency+WinStay+LoseShift+Area*(Session+FlexibilityIndex+PerserverationIndex+InitiationLatency+ChoiceLatency+RewardLatency+WinStay+LoseShift)+(1|RatID:Session)]						
Coefficients	**β**	SE	tStat	DF	P	CIL	CIU
Intercept	1.4433	0.4581	3.1505	25	0.0042	0.4998	2.3868
Initiation Latency	-0.1490	0.0700	-2.1278	25	**0.0434**	-0.2932	-0.0048
Choice Latency	0.0677	0.1210	0.5595	25	0.5808	-0.1814	0.3168
Reward Latency	0.1892	0.0840	2.2530	25	**0.0333**	0.0162	0.3621
WinStay	-2.0423	0.9446	-2.1622	25	**0.0404**	-3.9877	-0.0970
Area	-0.7024	0.2776	-2.5304	25	**0.0181**	-1.2741	-0.1307
LoseShift	-2.7002	1.6040	-1.6835	25	0.1047	-6.0037	0.6032
Flexibility Index	0.8666	0.8687	0.9976	25	0.3281	-0.9226	2.6557
Perseveration Index	3.7763	1.7935	2.1056	25	**0.0455**	0.0826	7.4700
Session	0.0087	0.0106	0.8186	25	0.4207	-0.0131	0.0305
Area:InitiationLatency	0.0946	0.0436	2.1676	25	**0.0399**	0.0047	0.1845
Area:ChoiceLatency	-0.0641	0.0902	-0.7109	25	0.4837	-0.2499	0.1217
Area:RewardLatency	-0.0971	0.0469	-2.0688	25	**0.0491**	-0.1938	-0.0004
Area:WinStay	1.5174	0.6084	2.4940	25	**0.0196**	0.2643	2.7704
Area:LoseShift	2.3028	0.9772	2.3565	25	**0.0266**	0.2902	4.3154
Area:Flexibility Index	-0.6076	0.5644	-1.0765	25	0.2920	-1.7701	0.5549
Area:Perseveration Index	-2.4325	1.1041	-2.2031	25	**0.0370**	-4.7065	-0.1585

Alpha Level 0.05

TABLE 17 (Table 16 Post-Hoc)

Post-Hoc Statistics on Area Interaction with M2 Lens Rats only **γ = Trial Outcome Decoder Accuracy in M2 Rats**							
Formula	γ~[1+PerseverationIndex+InitiationLatency+RewardLatency+WinStay+LoseShift+(1|RatID:Session)]						
Coefficients	**β**	SE	tStat	DF	P	CIL	CIU
(Intercept)	0.8398	0.1998	4.2042	12	0.0012	0.4046	1.2750
Initiation Latency	-0.0678	0.0281	-2.4183	12	**0.0324**	-0.1290	-0.0067
Reward Latency	0.0835	0.0398	2.0961	12	0.0579	-0.0033	0.1703
Win Stay	-0.2921	0.2255	-1.2951	12	0.2197	-0.7834	0.1993
Lose Shift	-0.1878	0.6896	-0.2723	12	0.7901	-1.6903	1.3148
Perseveration Index	0.9463	0.8409	1.1254	12	0.2824	-0.8858	2.7785

Post-Hoc Statistics on Area Interaction with OFC Lens Rats only **γ = Trial Outcome Decoder Accuracy in OFC Rats**							
Formula	γ~[1+PerseverationIndex+InitiationLatency+RewardLatency+WinStay+LoseShift+(1|RatID:Session)]						
Coefficients	**β**	SE	tStat	DF	P	CIL	CIU
(Intercept)	0.0749	0.1868	0.4007	18	0.6934	-0.3176	0.4674
Initiation Latency	0.0193	0.0151	1.2789	18	0.2172	-0.0124	0.0509
Reward Latency	-0.0069	0.0236	-0.2919	18	0.7737	-0.0564	0.0426
Win Stay	0.6517	0.2268	2.8730	18	**0.0101**	0.1751	1.1283
Lose Shift	1.5504	0.5505	2.8161	18	**0.0114**	0.3937	2.7070
Perseveration Index	-1.5430	0.6310	-2.4452	18	**0.0249**	-2.8687	-0.2172

Alpha Level 0.05.